JOC*Article*

Thermal Decomposition of Decalin: An *Ab Initio* Study

Kyungchan Chae and Angela Violi*

Department of Mechanical Engineering, The University of Michigan, Ann Arbor, Michigan 48109-2125

avioli@umich.edu

Received November 11, 2006

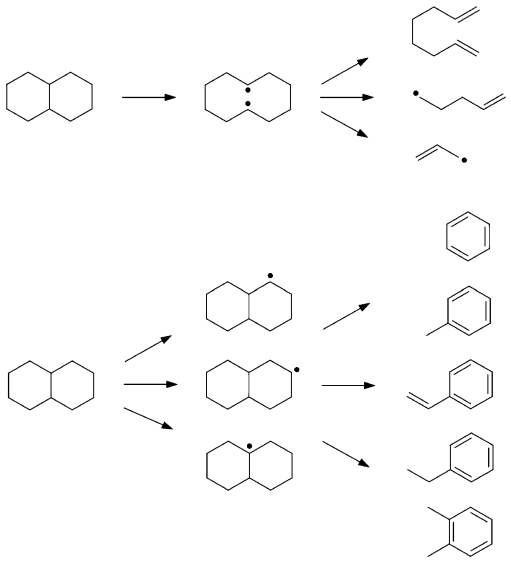

Density functional theory calculations (B3LYP and BH&HLYP functionals) of the potential energy surface have been performed to investigate the mechanisms of decalin breakdown, and the Rice−Ramsperger−Kassel−Marcus and transition state theory methods have been used to compute the high-pressure limit thermal rate constants for the new reaction pathways. The new pathways connect decalin to five primary monoaromatic species: benzene, toluene, styrene, ethylbenzene, and xylene. The reactions used for the new routes are carbon−carbon bond cleavage reaction, dissociation reaction, and hydrogen abstraction and addition reactions. A kinetic analysis was performed for pyrolytic conditions, and benzene, toluene, and xylene were identified as major products.

Introduction

Practical jet fuels, i.e., those fuels derived from the refinery processing of crude petroleum are chemically complex, often containing thousands of compounds. Because these fuels must meet broadly defined specifications, their composition varies not only with refinery and crude oil source but also with season and year of production. Moreover, composition changes as the fuel ages. As a result, it is difficult to control the consistency in fuel composition required for the purpose of research.

The use of surrogate blend, comprised of a relatively small number of high purity hydrocarbons and blended to simulate the combustion performance of practical fuel, has the advantage of allowing fuel composition to be accurately controlled and monitored.[1] In addition to providing a model fuel for the study of the effect of fuel properties and chemical composition on combustor performance, the compositional control afforded by a surrogate fuel is attractive for the development and verification of computational codes for combustor design. Surrogate mixtures are desirable for experimental and computational tractability and reproducibility. The type of surrogate mixture used is dependent ideally upon the fuel properties that are being simulated: surrogates may be tailored to reproduce the physical, chemical, or more comprehensive behavior of a fuel in a given application. A physical surrogate is designed to reproduce physical properties such as density, thermal conductivity, heat capacity, viscosity, surface tension, and volatility. A chemical

(1) Cookie, J. A.; Bellucci, M.; Smooke, M. D.; et al. Proceedings of the Combustion Institute 30, Part 1, 2005, pp 439−446.

10.1021/jo062324x CCC: $37.00
Published on Web 03/30/2007

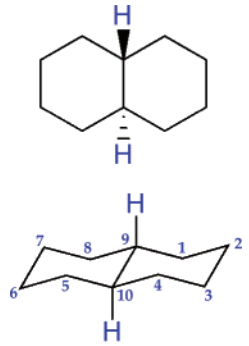

FIGURE 1. *trans*-Decalin.

surrogate, on the other hand, has similar hydrocarbon types and distribution, and it reproduces chemical properties such as oxidation stability, ignition temperature, rates of reaction, and sooting behavior.[2−5]

The major categories of hydrocarbons in jet fuels are alkanes, cycloalkanes (naphthenes), aromatics, and alkenes.[3] Alkanes (such as dodecane, tetradecane, heptane, decane, and isooctane) are the most abundant components in real fuels and account for 50−60% of the fuel by volume. Naphthenes (such as methylcyclohexane, tetralin, and decalin) and aromatics (such as toluene and xylene) represent 20−30% by volume. Alkenes account for less than 5%.[4−7]

While the kinetic properties of normal and branched alkanes have been already studied and applied to different systems,[8,9] the kinetic modeling of aromatics and especially naphthenes are less defined because of their complex reaction mechanisms and large number of possible reactions.

Prompted by this need, in this paper we report on the breakdown mechanism for decalin ($C_{10}H_{18}$), representative of the naphthene class (Figure 1). Decahydronaphthalene, also known as decalin, is a bicyclic organic compound. It is the saturated analogue of naphthalene and can be prepared from it by hydrogenation in a fused state in the presence of a catalyst. Decalin occurs in *cis* and *trans* forms. The *trans* form is energetically more stable because of less steric interactions.

Gollis et al.[10] evaluated pure hydrocarbons as potential jet fuels and they showed that decalin has the highest thermal stability among the compounds considered. In addition, decalin can decompose to gas without forming deposits so that it can be used at high temperatures.[11] This is one of the critical characteristics required for an advanced jet fuel.[12,13]

Decalin also has an attractive feature as potential hydrogen donor to suppress pyrolytic deposits. By donating hydrogen atoms to the radicals formed during the thermal decomposition process, hydrogen donor additives help to prevent the formation of various thermal deposits. Decalin, at 1.0% by volume, reduced pyrolytic deposits by 50% relative to the baseline fuel.[14−17] For these reasons, great interest is devoted to the use of decalin for surrogate jet fuels as well as an advanced fuel additive to suppress fuel deposits.

Decalin has been employed as a reference component of the multiring naphthene class for JP-8 surrogates.[3−6,18] Surrogates with 35% by volume of decalin showed good agreement with experimental results on sooting tendency of pool fire. Agosta et al.[6] have included 6% by volume of decalin in their surrogate to match the autoignition and combustion behavior hydrocarbon fuel.

In this paper we perform a detailed analysis of the reaction mechanisms for decalin pyrolysis using density functional theory calculations. Reaction rates are computed for the pathways analyzed together with the thermodynamic data of all the intermediates involved in the reaction steps. After the first two sections that describe the breakdown routes for decalin, the reaction pathways identified are implemented in a Chemkin-type kinetic mechanism to simulate a pyrolytic environment.

Computational Method

Geometries and frequencies of the reactants, transition states, and products were calculated by using the hybrid density functional B3LYP method (i.e., Becke's three-parameter non local exchange functional[19] with the non local correlation function of Lee, Yang, and Parr,[20−21] with the 6-31G(d,p) basis set. Single-point energy calculations for all transition state geometries were performed using the BH&HLYP/6-31G(d,p) level of theory, which predicts barrier heights more accurately than the B3LYP method, particularly for the hydrogen abstraction reactions.[22−25] Transition structures (TS) were identified by the existence of only a singular imaginary frequency in the normal mode coordinate analysis, an evaluation of the TS geometry, and the reaction coordinate's vibrational motion. The frequency calculations also allowed the zero-point energy (ZPE) corrections to be obtained. Intrinsic reaction coordinate calculations were carried out to guarantee that the transition states found indeed connect the reactant and product of the reaction step. All computations were done by using the Gaussian 03 program.[26]

(2) Edwards, T.; Maurice, L. Q. *J. Propul. Power* **2001**, *17* (2), 461−466.
(3) Violi, A.; Yan, S.; Eddings, E. G.; et al. *Combust. Sci. Technol.* **2002**, *174* (11−2), 399−417.
(4) Ranzi, E. *Energy Fuels* **2006**, *20* (3), 1024−1032.
(5) Schulz, W. D. *Prepr.*—Am. Chem. Soc., Div. Pet. Chem. **1991**, *37* (2), 383−392.
(6) Agosta, A.; Cernansky, N. P.; Miller, D. L.; Faravelli, T.; Ranzi, E. *Exp. Therm. Fluid Sci.* **2004**, *28* (7), 701−708.
(7) Montgomery, C. J.; Cannon, S. M.; Mawid, M. A.; Sekar, B. 40th AIAA Aerospace Sciences Meeting, Reno, NV, January 2002, Paper No. 2002−0336.
(8) Westbrook, C. K.; Pitz, W. J.; Curran, H. C.; Boercker, J.; Kunrath, E. *Int. J. Chem. Kinet.* **2001**, *33* (12), 868−877.
(9) Axelsson, E. I.; Brezinsky, K.; Dryer, F. L.; Pitz, W. J.; Westbrook, C. K. 21th International Symposium on Combustion, 1986.
(10) Gollis, M. H.; Belenyessy, L. I.; Gudzinowicz, B. J.; Koch, S. D.; Smith, J. O.; Wineman, R. J. *J. Chem. Eng. Data* **1962**, *7* (2), 311−316.
(11) Corporan, E.; Minus, D. K.; Williams, T. F. 35th AIAA Joint conference, June 1999, 99−2213.
(12) Edwards, T.; Harrison, W. E.; Schobert, H. H. *AIAA* **1997**, 97−2848.
(13) Maurice, L. Q.; Lander, H.; Edwards, T.; Harrison, W. E. *Fuel* **2001**, *80*, 747−756.
(14) Song, C.; Lai, W. C.; Schobert, H. H. *Ind. Eng. Chem. Res.* **1994**, *33* (3), 548−557.
(15) Yoon, E. M.; Selvaraj, L.; Song, c.; Stallman, J. B.; Coleman, M. M. *Energy Fuels* **1996**, *10*, 806−811.
(16) Corporan, E.; Minus, D. K. *AIAA* **1998**, 98−3996.
(17) Maurice, L. Q.; Corporan, E.; Minus, D.; Mantz, R.; Edwards, T.; Wohlwend, K.; Harrison, W. E.; Striebich, R. C.; Sidhu, S.; Graham, J.; Hitch, B.; Wickham, D.; Karpuk, M. *AIAA* **1999**, 99−4916.
(18) Eddings, E. G.; Yan, S.; Ciro, W.; Sarofim, A. F. *Combust. Sci. Technol.* **2005**, *177*, 715−739.
(19) Becke, A. D. *J. Chem. Phys.* **1992**, *96*, 2155; **1992**, *97*, 9173; **1993**, *98*, 5648.
(20) Lee, C.; Yang, W.; Parr, R. G. *Phys. Rev. B* **1988**, *37*, 785.
(21) Hebre, W.; Radom, L.; Schleyer, P. R.; Pople, J. A. *Ab initio Molecular Orbital Theory*; Wiley: New York, 1986.
(22) Wang, D.; Violi, A. *J. Org. Chem.* **2006**, *71* (22), 8365−8371.
(23) Wang, D.; Violi, A.; Kim, D. H.; et al. *J. Phys. Chem. A* **2006**, *110* (14), 4719−4725.
(24) Violi, A. *J. Phys. Chem. A* **2005**, *109* (34), 7781−7787.
(25) Violi, A.; Truong, T. N.; Saforim, A. F. *J. Phys. Chem. A* **2004**, *108* (22), 4846−4852.

First-order thermal rate constants at the high-pressure limit were computed using the Rice−Ramsperger−Kassel−Marcus (RRKM) theory.[27−29] For bimolecular reactions, the transition state theory (TST) was employed to calculate second-order rate constants. Nonlinear Arrhenius effects resulting from changes in the thermochemical properties of the respective transition state relative to those of its adduct with temperature were incorporated using a two-parameter Arrhenius pre-exponential factor (A, n) in AT^n. All the rate constants of the reaction steps of each pathway were calculated using TheRate code[30] (THEoretical RATEs). The transmission coefficients which account for the quantum mechanical tunneling effect were calculated using the Eckart method.[31]

The thermal rate coefficient is expressed as

$$k(T) = \kappa(T)\sigma \frac{k_B T}{h} \frac{Q^{\ddagger}(T)}{\Phi^{R}(T)} e^{-\Delta V^{\ddagger}/k_B T}$$

where κ is the transmission coefficient accounting for the quantum mechanical tunneling effects, σ is the reaction symmetry number, $Q\dagger(T)$ and $\Phi^R(T)$ are the total partition functions (per unit volume) of the transition state and reactant, respectively, $\Delta V\dagger$ is the classical barrier height, T is the temperature, and k_B and h are the Boltzmann and Planck constants, respectively.

To asses the suitability of the B3LYP/6-31G(d,p) level of theory for studies of reactions involving aryl radicals and arynes, we performed comparisons with experimental data available for compounds that belong to those classes. Thus, the B3LYP/6-31G-(d,p) C−H bond dissociation energy (BDE) of benzene equals 110.17 kcal/mol at $T = 0$ K, in agreement with the recent experimental values of 109.8 ± 0.8 kcal/mol[32] and 112.0 ± 0.6 kcal/mol.[33]

The energies and barriers quoted in this paper pertain to $T =$ 0 K and include zero-point energies.

Results and Discussion

Experimental results previously reported on decalin pyrolysis at high temperature[34−36] have shown that the most probable initiation steps of thermal cracking are the carbon−carbon (C_9−C_{10}) bond cleavage (Figure 2a) and hydrogen abstraction (from C_1, C_2, C_9) reactions (Figure 2b). In addition, experimental data on thermal decomposition of decalin carried out under near critical and supercritical conditions indicated the interconversion between *cis*- and *trans*-decalin and identified toluene, 1-butylcyclohexene, and 1-methylcyclohexene as products.[37] Billaud et al. reported detailed experimental results on the thermal cracking of decalin in a steam pyrolysis environment[38] and measured the relative abundance of some aromatics, such as benzene, toluene, and styrene.

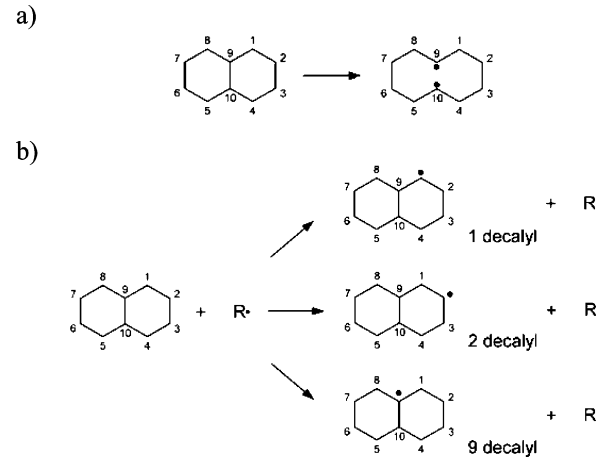

FIGURE 2. Initiation reactions: (a) carbon−carbon bond cleavage and (b) hydrogen abstractions.

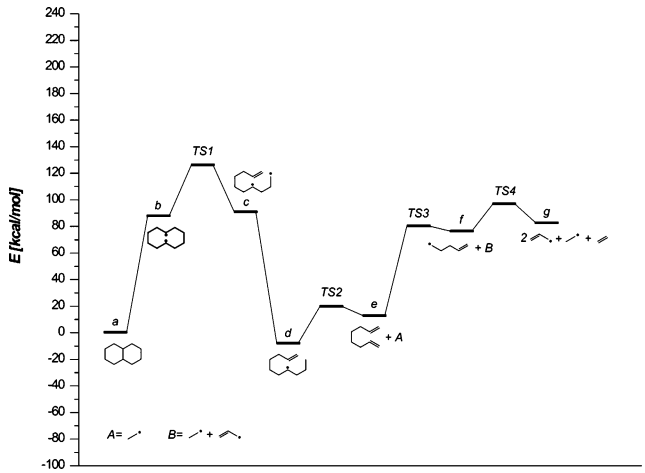

FIGURE 3. Potential energy diagrams involving the C_9–C_{10} bond cleavage.

Drawing on these experimental evidence, we identified a series of new reaction pathways leading to the formation of smaller hydrocarbons, such as toluene, benzene, styrene, ethylbenzene, and xylene.

A. Carbon−Carbon Bond Cleavage.

A.1. Initiation Reaction. Figure 3 shows the potential energy surface for the breakdown of decalin through C_9–C_{10} bond cleavage. No transition state was identified to produce intermediate **b** (first-order saddle point), and the reaction energy for **a** → **b** is 88.02 kcal/mol. Further C−C bond cleavage leads to the formation of **c** with an energy barrier of 38.11 kcal/mol.

(26) *Gaussian 03, Revision C.01*; Frisch, M. J.; Trucks, G. W.; Schlegel, H. B.; Scuseria, G. E.; Robb, M. A.; Cheeseman, J. R.; Montgomery, J. A., Jr.; Vreven, T.; Kudin, K. N.; Burant, J. C.; Millam, J. M.; Iyengar, S. S.; Tomasi, J.; Barone, V.; Mennucci, B.; Cossi, M.; Scalmani, G.; Rega, N.; Petersson, G. A.; Nakatsuji, H.; Hada, M.; Ehara, M.; Toyota, K.; Fukuda, R.; Hasegawa, J.; Ishida, M.; Nakajima, T.; Honda, Y.; Kitao, O.; Nakai, H.; Klene, M.; Li, X.; Knox, J. E.; Hratchian, H. P.; Cross, J. B.; Bakken, V.; Adamo, C.; Jaramillo, J.; Gomperts, R.; Stratmann, R. E.; Yazyev, O.; Austin, A. J.; Cammi, R.; Pomelli, C.; Ochterski, J. W.; Ayala, P. Y.; Morokuma, K.; Voth, G. A.; Salvador, P.; Dannenberg, J. J.; Zakrzewski, V. G.; Dapprich, S.; Daniels, A. D.; Strain, M. C.; Farkas, O.; Malick, D. K.; Rabuck, A. D.; Raghavachari, K.; Foresman, J. B.; Ortiz, J. V.; Cui, Q.; Baboul, A. G.; Clifford, S.; Cioslowski, J.; Stefanov, B. B.; Liu, G.; Liashenko, A.; Piskorz, P.; Komaromi, I.; Martin, R. L.; Fox, D. J.; Keith, T.; Al-Laham, M. A.; Peng, C. Y.; Nanayakkara, A.; Challacombe, M.; Gill, P. M. W.; Johnson, B.; Chen, W.; Wong, M. W.; Gonzalez, C.; Pople, J. A. Gaussian, Inc.: Wallingford, CT, 2004.

(27) Gillespie, D. T. *J. Phys. Chem.* **1977**, *81*, 2340−2361.

(28) Gillespie, D. T. *J. Comput. Phys.* **1976**, *22*, 403−404.

(29) Gillespie, D. T. *J. Comput. Phys.* **1978**, *28*, 395−407.

(30) Ducan, W. T.; Bell, R. L.; Truong, T. N. *J. Phys. Chem. A* **2003**, *107*, 782.

(31) Truong, T. N.; Truhlar, D. G. *J. Chem. Phys.* **1990**, *93*, 1761.

(32) Berkowitz, J.; Ellison, G. B.; Gutman, D. *J. Phys. Chem.* **1994**, *98*, 2744.

(33) Davico, G. E.; Bierbaum, V. M.; DePuy, C. H.; Ellison, G. B.; Squires, R. R. *J. Am. Chem. Soc.* **1995**, *117*, 2590.

(34) Hillebrand, W.; Hodek, W.; Kolling, G. *Fuel* **1984**, *63*, 756−761.

(35) Ondruschka, B.; Zimmermann, G.; Remmler, M.; Sedlackova, M.; Pola, J. *J. Anal. Appl. Pyrolysis* **1990**, *18*, 19−32.

(36) Ondruschka, B.; Zimmermann, G.; Zeigler, U. *J. Anal. Appl. Pyrolysis* **1990**, *18*, 33−39.

(37) Yu, J.; Eser, S. *Ind. Eng. Chem. Res.* **1998**, *37*, 4601−4608.

(38) Billaud, F.; Chaverot, P.; Freund, E. *J. Anal. Appl. Pyrolysis* **1987**, *11*, 39−53.

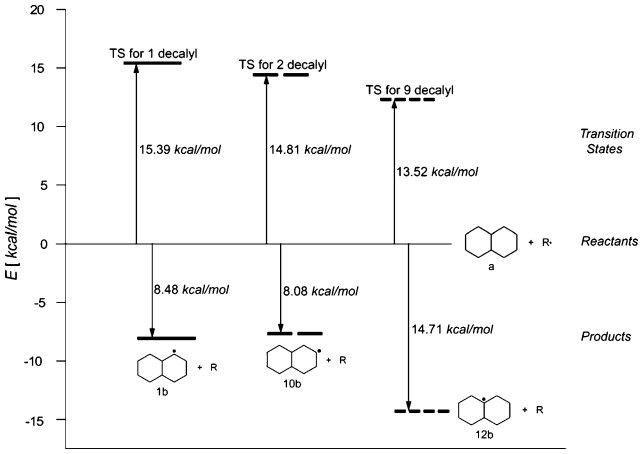

FIGURE 4. Energy barriers to produce 1-, 2-, and 9-decalyl.

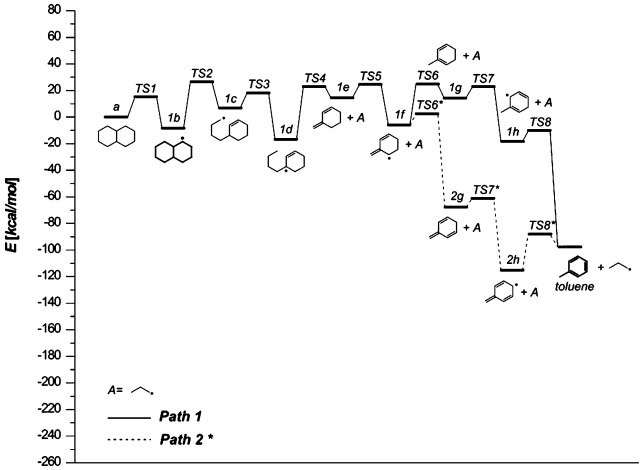

FIGURE 5. Potential energy diagrams for paths 1 and 2.

A.2. Propagation Steps. The addition of hydrogen to the biradical **c** produces intermediate **d**, without any transition barrier. Radical **d** undergoes C−C scission breaking two carbons away from the charged carbon producing C_2H_5 and **e**, which has two fewer carbon atoms. The energy barrier for this step is 27.67 kcal/mol. Subsequent C−C scission leads to the formation of C_5H_9 radical (**f**) and C_3H_5, followed by the formation of allyl radical (**g**) and ethylene.

B. Carbon−Hydrogen Bond Breaking.

B.1. Initiation Reaction. Figure 4 reports the initiation steps for the formation of 1-, 2-, and 9-decalyl through H abstraction by radical species R•. The results showed in Figure 4 are relative to hydrogen abstraction reactions by CH_3•. The energy barrier to produce 1-decalyl is 15.39 kcal/mol, higher than the values computed for 2-decalyl and 9-decalyl, which are 14.81 and 13.52, respectively.

B.2. Propagation Steps.

B.2.a. 1-Decalyl Radical. From 1-decalyl (**1b**) we identified nine pathways leading to the formation of various aromatics including benzene, styrene, and xylene. Paths 1−6 begin with the C_8-C_9 bond cleavage, and paths 7−9 begin with the C_2-C_3 bond cleavage.

Figure 5 reports paths 1 and 2 to form toluene (C_7H_8) and propyl (C_3H_7). The energy barrier for the formation of radical **1c** is 34.62 kcal/mol and the following hydrogen migration to produce **1d** has transition energy of 11.32 kcal/mol. Subsequently, **1d** decomposes to form **1e** and propyl radical (**1d** → **1e** reaction). Hydrogen abstraction from intermediate **1e** produces radical **1f** with transition energy of 10.10 kcal/mol. From **1f** two different pathways have been identified that lead to the formation of toluene. The **1f** → **1g**, **1g** → **1h**, and **1h** → **toluene** route (path 1) involves hydrogen addition, abstraction, and further addition to produce toluene. From intermediate **1f** the most significant barrier is represented by **1f** → **1g**, being 31.21 kcal/mol.

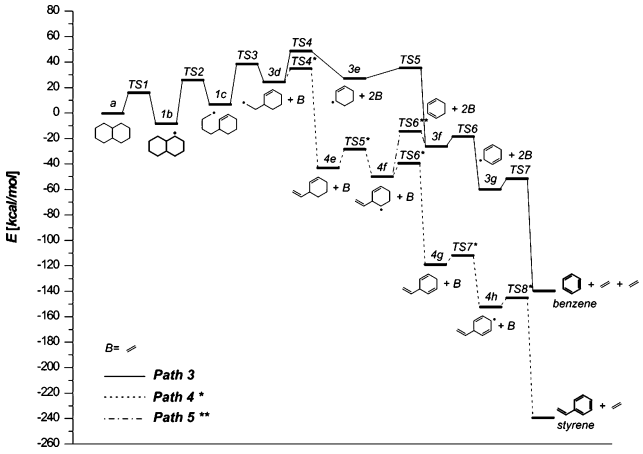

FIGURE 6. Potential energy diagrams for paths 3, 4, and 5.

In path 2, **1f** undergoes two hydrogen abstraction reactions (**1f** → **2g** and **2g** → **2h**) and hydrogen addition (**2h** → **toluene**) to produce toluene. The energy barriers involved in this route are lower than the ones in path 1, and the intermediates formed are very stable.

Figure 6 shows three reaction pathways (paths 3−5) to produce benzene (C_6H_6) and styrene (C_8H_8) starting from 1-decalyl (**1b**). From intermediate **1c**, **3d** and **3e** are formed through two subsequent β-scission reactions in which the radical breaks two carbons away from the charged carbon producing an olefin (ethylene) and a primary free radical, which has two fewer carbon atoms. The energy barriers of these reactions are 30.97 kcal/mol for **1c** → **3d** and 22.48 kcal/mol for **3d** → **3e**. Sequential hydrogen abstraction reactions (**3e** → **3f**, **3f** → **3g**, and **3g** → **benzene**) lead to the formation of benzene (path 3).

As an alternative, **3d** can undergo hydrogen abstraction to form **4e**. Styrene is then produced through hydrogen abstraction reactions (**3d** → **4e** → **4f** → **4g** → **4h** → **styrene**) (path 4).

Decomposition of **4f** into **3f** and vinyl radical (C_2H_3•) represent another reaction pathway to form benzene (path 5). The energy barrier for **4f** → **3f** is 35.56 kcal/mol, higher than the one for **3d** → **3e** reaction (22.48 kcal/mol). Benzene is then formed from **3f** following path 3 previously described.

Ethylbenzene (C_8H_{10}) is produced through path 6 reported in Figure 7. Intermediate **3d** undergoes hydrogen addition to produce **6e** with an energy barrier of 20.92 kcal/mol energy. Subsequent hydrogen abstractions (**6e** → **6f** → **6g** → **6h** → **ethylbenzene**) produce ethylbenzene.

Figure 8 shows paths 7 and 8 forming benzene and styrene as main polycyclic aromatic hydrocarbons. Radical **1b** undergoes C_2-C_3 bond cleavage to produce **7c**. This reaction has an energy barrier of 35.37 kcal/mol similar to the C_8-C_9 cleavage reaction of path 1 (34.62 kcal/mol). Two successive decomposition reactions to produce first ethylene (C_2H_4) and **7d** and then vinyl radical and intermediate **7e** (**7d** → **7e**) are the peculiar steps of this pathway.

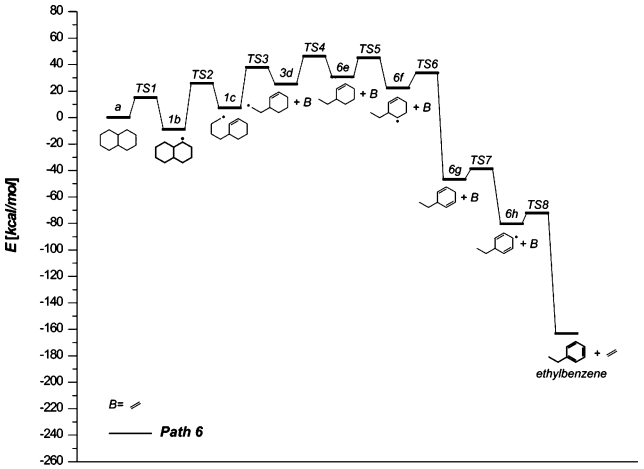

FIGURE 7. Potential energy diagram for path 6.

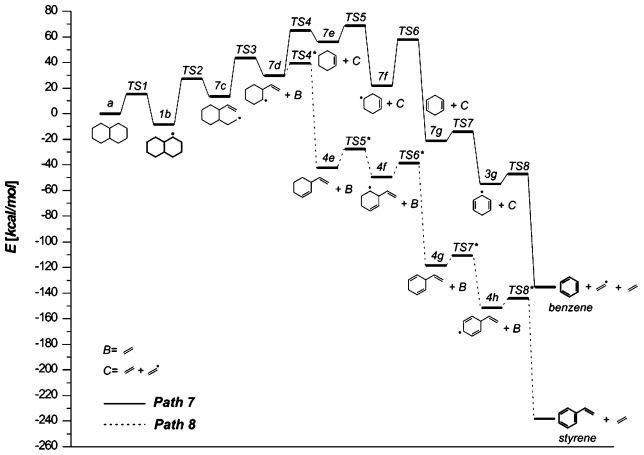

FIGURE 8. Potential energy diagrams for paths 7 and 8.

The energy barrier for **7c** → **7d** is 29.34 kcal/mol very similar to that of **1c** → **3d** of path 3 (30.97 kcal/mol) but the **7d** → **7e** reaction shows a high-energy barrier, 35.49 kcal/mol. Subsequent hydrogen abstraction reactions (**7e** → **7f** → **7g** → **3g** → **benzene**) produce benzene.

Pathway 8 proceeds from intermediate **7d** through hydrogen abstraction reactions (**7d** → **4e** → **4f** → **4g** → **4h** → **styrene**) to form styrene.

Figure 9 reports the last decomposition pathway for 1-decalyl radical. Intermediate **7c** undergoes hydrogen addition and abstraction to produce radical **9e**. The energies for **7c** → **9d** and **9d** → **9e** are 22.46 kcal/mol and 14.75 kcal/mol, respectively. Intermediate **9e** decomposes to vinyl radical and **9f** (**9e** → **9f**, 34.88 kcal/mol energy barrier). Ethylbenzene is then produced through hydrogen abstraction reactions.

B.2.b. 2-Decalyl Radical. Figure 10 reports the reaction pathway for the decomposition of 2-decalyl. The sequence begins with C_3-C_4 bond cleavage (**10b** → **10c**) to form **10c** that then undergoes hydrogen addition and abstraction to produce **10e**. An energy barrier of 17.81 kcal/mol is then required to decompose **10e** into **10f** and allyl radical (C_3H_5). Hydrogen abstraction reactions (**10f** → **10g** → **10h** → **10i** → **toluene**) lead to the formation of toluene (path 10)

Intermediate **10b** can produce **11c** through C_1-C_9 bond cleavage. The energy barrier for this reaction (34.64 kcal/mol) is slightly lower than that of **10b** → **10c** (37.47 kcal/mol).

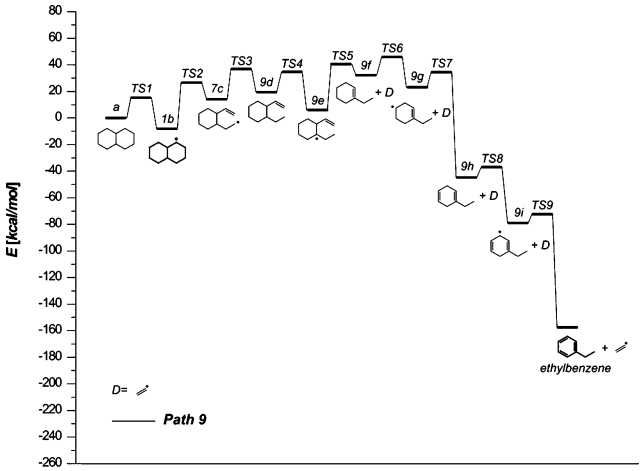

FIGURE 9. Potential energy diagram for path 9.

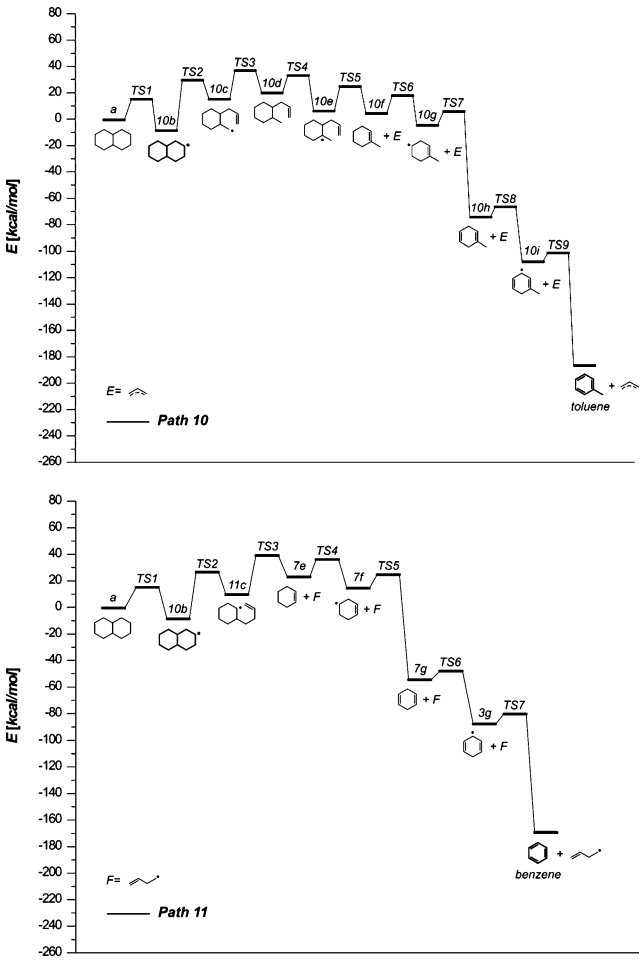

FIGURE 10. Potential energy diagrams for path 10 (upper panel) and path 11 (lower panel).

Intermediate **11c** undergoes a decomposition reaction to produce C_4H_7 and intermediate **7e**, (**11c** → **7e**). From **7e** the pathway is analogous to path 7 leading to the formation of benzene.

B.2.c. 9-Decalyl Radical. The reaction pathways for 9-decalyl radical are reported in Figure 11. The C_1-C_2 bond cleavage reaction (**12b** → **12c**) requires 34.04 kcal/mol to overcome the energy barrier and produce intermediate **12c**. This isomer radical (**12c**) undergoes a decomposition reaction (**12c** → **12d**), to form

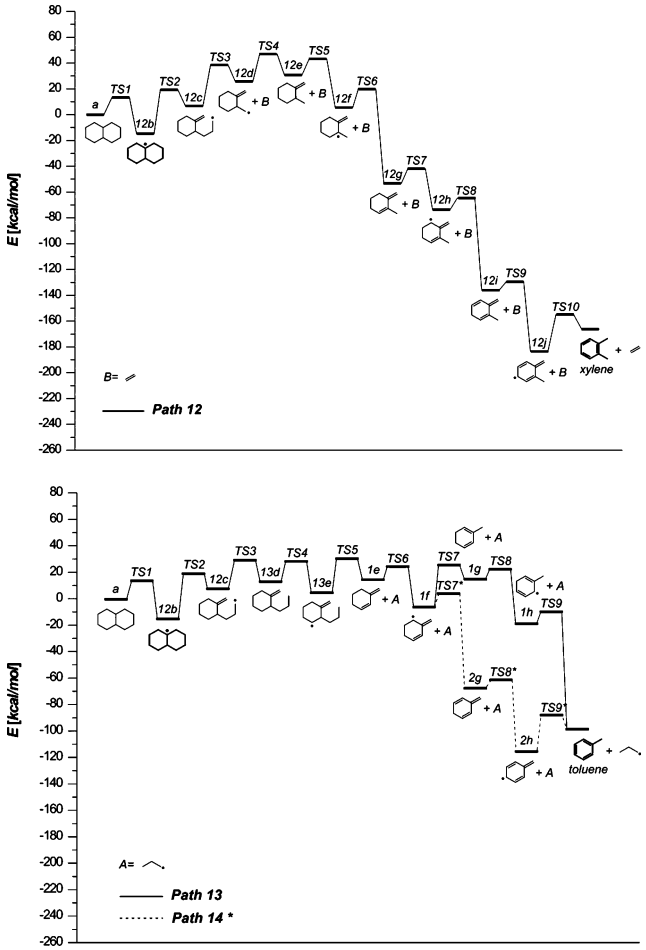

FIGURE 11. Potential energy diagrams for path 12 (upper panel) and paths 13 and 14 (lower panel).

12d and ethylene. Successive hydrogen abstraction and addition reactions lead to the main aromatic identified in this pathway xylene (C_8H_{10}) (path 12, upper panel).

Alternatively, intermediate **12c** can undergo hydrogen addition (**12c** → **13d**, 21.87 kcal/mol) and abstraction (**13d** → **13e**, 14.86 kcal/mol) to produce intermediate **13e**—path 13. Propyl and intermediate **1e** are then formed from the decomposition of **1e**. From **1e** toluene is produced following the same reaction route described in paths 1 and 2 (lower panel).

Optimized Cartesian coordinates of all species involved in the reactions considered in this paper are reported in the Supporting Information along with vibrational frequencies, ZPE corrections, and moments of inertia.

The energy barriers and reaction energies for the pathways described above are collected in the Supporting Information Tables S1−S13. The energy values listed in the tables include the compensation of zero-point energies by their frequency calculations. For the transition states, the zero-point energies calculated using the BH&HLYP method were used.

Kinetic Modeling

Using the RRKM and TST computed high-pressure limit constants reported in Tables S1−S13, we performed kinetic modeling calculations of decalin pyrolysis. Considering that B3LYP/6-31G(d,p)//BH&HLYP/6-31G(d,p) frequencies and chemically accurate barriers and reaction energies were utilized in the rate calculations, we expect the resulting thermal rate constants to be of reasonable accuracy, as long as the high-pressure limit adequately describes the reaction conditions.

For the flame combustion at ambient conditions ($P \sim 1$ atm) the high-pressure limit approximation is generally warranted, and therefore our computed rate constants can be used in detailed kinetic modeling of atmospheric combustion.

The newly identified reaction pathways for decalin breakdown and their relative reaction rates were implemented in a kinetic mechanism analysis. For this calculation, we used the CHEMKIN software package[39,40] to study the time-dependent chemical kinetics behavior of a closed homogeneous gas mixture system (1 atm, 700∼1500 K). The mechanism includes all the reaction steps previously described. Table 1 reports the calculated product yields (%) of benzene, toluene, styrene, ethylbenzene, and xylene as a function of temperature.

At low-temperature conditions (∼700 K) the major reaction product is benzene, which is formed mainly through pathways 3, 7, and 11. Route 11 accounts for most of the benzene production within the temperature ranges considered: at 700 K pathway 11 contributes 99% to benzene production, and the value goes down to 76% at 1500 K. The contribution of pathways 3 and 7 to benzene formation increases with temperature, reaching 8.55% and 14.69% at 1500 K, respectively.

Toluene is produced through pathways 1 and 2. The other three routes (pathways 10, 13, and 14) leading to toluene are less significant: pathways 13 and 14 compete with pathway 12 to form xylene, and pathway 10 overcomes path 11 to produce benzene. At low temperatures toluene is mainly formed through pathway 2 (99%), but as the temperature increases the contribution of pathway 2 becomes significant. At 1500 K, pathway 1 contributes 67% and pathway 2 32% to the final yields of toluene.

The benzene production reaches a minimum at 1000 K where the toluene yield peaks. The formation of these two compounds is highly intertwined, and it is the result of the competition of pathway 1 and 7 in which intermediate **1b** can form **1c** (leading to toluene) or **7c** to produce benzene.

Styrene is produced through pathway 8, and the overall yield is low compared with benzene and toluene. This is due to the competition with pathways 3 and 7 that lead to the formation of benzene.

Ethylbenzene is formed through paths 6 and 9. At low temperatures, path 9 represents the main production route for ethylbenzene. At 1500 K, pathway 6 accounts for 10% of the total yield with the remaining being part of pathway 9. In the same way as styrene, ethylbenzene is not one of the main products due to the competition with pathways 3 and 7.

Xylene is produced through pathway 12, and its yield increases as the temperature goes up. Its production, however, is below 1% in the temperature range analyzed, indicating that xylene is a minor product of decalin breakdown.

The results of our calculations of potential energy surface for decalin and subsequent modeling predicts yields of benzene, styrene, xylene, and ethylbenzene at various temperatures. We

(39) Lutz, A. E.; Kee, R. J.; Miller, J. A. *SENKIN: A Fortran program for predicting homogeneous gas phase chemical kinetics with sensitivity analysis*; Sandia National Laboratories Report No. SAND-87-8248; Sandia National Laboratories: Albuquerque, NM, 1988.

(40) Kee, R. J.; Rupley, F. M.; Miller, J. A. *CHEMKIN 2: A Fortran Chemical kinetics Package for the analysis of gas phase chemical kinetics*; Sandia National Laboratories Report No. SAND-89-8009B; Sandia National Laboratories: Albuquerque, NM, 1989.

TABLE 1. Calculated Product Yields (%) of Benzene, Toluene, Styrene, Ethylbenzene, and Xylene as a Function of Temperature

	temperature (*K*)								
species	700	800	900	1000	1100	1200	1300	1400	1500
	relative yields of products								
benzene (C_6H_6)	93.73	84.18	70.81	68.42	71.37	75.13	78.79	81.91	84.68
toluene (C_7H_8)	6.25	15.81	29.17	31.47	28.44	24.60	20.86	17.64	14.78
styrene (C_8H_8)	0.02	0.0004	~0	~0	~0	~0	~0	~0	~0
xylene (C_8H_{10})	~0	0.0006	0.02	0.11	0.19	0.27	0.35	0.45	0.54
	contribution of each pathway to the products								
benzene									
path 3	0.03	0.13	0.41	1.03	2.01	3.33	4.91	6.70	8.55
path 7	0.26	1.12	2.93	5.95	9.07	11.52	13.10	14.10	14.69
path 11	99.71	98.75	96.66	93.02	88.92	85.15	81.99	79.20	76.76
toluene									
path 1	0.71	9.60	20.69	31.55	39.74	47.59	55.40	62.05	67.83
path 2	99.29	91.40	79.31	68.45	60.26	52.41	44.60	37.95	32.17
styrene									
path 8	100	100	100	100	100	100	100	100	100
ethylbenzene									
path 6	0.49	0.99	1.45	2.02	2.80	3.94	5.54	7.45	9.58
path 9	99.51	99.01	98.55	97.98	97.20	96.06	94.46	92.55	90.42
xylene									
path 12	100	100	100	100	100	100	100	100	100

expect that our RRKM and TST computed rate constants for the decalin breakdown can be further incorporated in existing kinetic schemes for flame combustion and pyrolysis to improve the prediction of aromatic concentrations. The data provided for the rate constants are fit to analytical expressions convenient for kinetic modeling.

Conclusions

The present study identifies possible reaction pathways that connect decalin molecule to five primary monoaromatic species: benzene, toluene, styrene, ethylbenzene, and xylene. The basic reactions for the new routes are carbon−carbon bond cleavage reaction, dissociation reaction, and hydrogen abstraction and addition reactions. The carbon bond cleavage reaction and hydrogen addition reaction have a high-energy barrier (30−40 kcal/mol) while the hydrogen abstraction reactions show a lower energy barrier (7−15 kcal/mol). The reaction rate calculations and kinetic mechanism analysis show that the main pathways for benzene production are 3, 7, and 11, while pathways 1 and 2 contribute to toluene. Pathway 12 produces xylene. The results also indicate that most of the hydrogen abstraction reactions from decalin molecule will produce the 2-decalyl and 1-decalyl radical. 1-Decalyl radical is very stable, and it represents the main radical produced from decalin.

Xylene molecule is produced only from 9-decalyl radical (path 12) and constitutes a small percentage of the product mixture. Benzene and toluene are produced through multiple pathways, and their concentrations in the products are significant. Styrene and ethylbenzene are also produced in small quantities.

The reaction mechanism produced in this work can be implemented in available mechanisms for modeling JP8 in order to build a complete description of the different surrogate.

Acknowledgment. The authors thank Prof. B. H. Schlegel for his insightful discussions and suggestions. This research is funded by the U.S. Air Force Scientific Office for Research (Grant FA9550-06-1-0376).

Supporting Information Available: Calculated total energies at the B3LYP level of theory, zero-point correction, vibrational frequencies, moment of inertia, and optimized Cartesian coordinates of all species involved in the studied mechanisms; RRKM and TST calculated high-pressure limit thermal rate constants for all studied reactions. This material is available free of charge via the Internet at http://pubs.acs.org.

JO062324X